RSC Advances

Chemical Communications

COMMUNICATION

A solvent additive to enhance the efficiency and the thermal stability of polymer : fullerene solar cells

L. Derue,[a] C. Lecourtier,[a,b] T. Gorisse,[a] L. Hirsch,[a] O. Dautel,[c] G. Wantz,[a]

[a] Univ. Bordeaux, IMS, UMR 5218, F-33400 Talence, France. E-mail: guillaume.wantz@ims-bordeaux.fr

[b] Solvay-RHODIA, LOF, UMR 5258, F-33600 Pessac, France.

[c] ICGM, AM2N, UMR 5253, F-34296 Montpellier, France. E-mail: olivier.dautel@enscm.fr

A novel bisazide molecule to be used in polymer-fullerene bulk heterojunction (BHJ) solar cells with two distinct functionalities is reported here. Firstly, it acts as a solvent-additive to reach optimized BHJ morphology and power conversion efficiencies without further requirements of annealing post-treatment of the active layer. Secondly, this molecule is a powerful thermally-triggered cross-linker for fullerenes enabling to freeze the BHJ morphology in its optimized form making active layers thermally stable.

Since the discovery of bulk-heterojunction polymer:fullerene solar cells in 1995[1], intensive research has been done towards the understanding and the control of the active layer morphology[2]. Prerequisite for efficient charge generation is that excitons are photogenerated near donor-acceptor interfaces with domains size of the range of excitons diffusion length. Presently, one can achieve such an optimized morphology with different processing tools such as thermal or solvent annealing of active layers[3] or by the use of solvent additives[4]. Among these technics, this latter is particularly attractive[5] for low-cost and large-scale production of organic solar cells. The effect of solvent additives have been attributed to two properties: their selective solubility towards one blend component and their higher boiling-point than the host solvent enabling morphological control of the active layer[6]. Following these guidelines, various kinds of solvent additive molecules have been reported[7,8]. Among them, one of the mostly used is 1,8-octanedithiol (ODT) with which efficiency of PCPDTBT:PC$_{71}$BM solar cells increased from 2,8% to 5,5%[4]. For the benchmark couple of materials, P3HT:PC$_{61}$BM system[9], efficiency of 2,4% was reported[10],Y. Yang and coworkers also demonstrated the use of ODT to allow a demixing between the two components into an optimized morphology[11]. Nevertheless, these optimal nano-sized phases segregated BHJ is a thermodynamically metastable system. It is well known that thermal treatment of P3HT:PC$_{61}$BM-based bulk heterojunction leads to the diffusion and the crystallization of PC$_{61}$BM molecules[12,13]. This micro-phase crystallization

decreases the overall interfacial area and hence the possibility for excitons dissociation between P3HT and PC$_{61}$BM which is critical for photovoltaic devices performances. Indeed, Manca *and coworkers* have shown PC$_{61}$BM micro-crystals formation after only 5 minutes at 125°C.[14] Recently, we reported similar phenomenon for thermal ageing carried out at 85°C [15] as a standard temperature for solar cells ageing.[16] Thermal stabilization of polymer:fullerene-based bulk-heterojunction solar cells is therefore essential. One way for suppressing the micro-sized phase segregation is to cross-link molecules inside the active layer once the optimized BHJ morphology is achieved [17]. Different cross-linkable functions such as oxetane[18], bromide[19], anthracene[20], cinnamate[21] or azide[22] were reported. In previous work, we have already reported that bisazide-based crosslinkers reacting by cycloaddition on fullerene derivatives triggered at low temperature (80°C) can be used to stabilize of donor-acceptor bulk heterojunctions[15]. However, the optimized BHJ morphology had to be achieved prior to crosslinking using solvent additives such as DIO or ODT for instance. Based on this concept, we present here a new specifically designed cross-linker, 1,10-diazidodecane (**DAD**, Figure 1) which meets a twofold objective : efficiency enhancement similar to solvent additive effect (ODT) and thermal stabilization of P3HT:PC$_{61}$BM-based solar cells. We first demonstrate that adding **DAD** into a P3HT:PC$_{61}$BM solution increases the degree of P3HT crystallinity after spin-coating and provides an optimized morphology for efficient photovoltaic devices. Secondly, we demonstrate the effective thermal stabilization of the optimal bulk heterojunction thanks to crosslinking.

Figure 1a shows the UV-Visible absorption spectroscopy of P3HT:PC$_{61}$BM films processed with various volume ratio of 1,10-diazidodecane as an additive. The films are obtained by spin-coating the blend solution at 1000 rpm for 60 s and let to dry at room temperature without further color change after deposition as a sign of spontaneous organization of materials. Compared to the P3HT:PC$_{61}$BM spectrum without additive (black curve), the incorporation of DAD in the blend exhibits a

red-shift absorption of the polymer spectrum highlighted by the three well-known vibronic features of P3HT. The first two bands (at 510 nm and 550 nm) are attributed to the π-π* transition and the shoulder at 600 nm is due to the inter-chain interactions[23]. For comparison, films were processed with 1,8-octanedithiol (ODT) and shown in Figure 1b. The effect of ODT on the absorption spectra of P3HT is similar to the one achieved with DAD. As a result, the addition of DAD significantly enhances light harvesting. Figure 2 outlines the photovoltaic parameters of P3HT:$PC_{61}BM$ solar cells as a function of DAD content. Before thermal ageing (black symbols), P3HT:$PC_{61}BM$ solar cells show low efficiency of 0.66 % due to a non-optimal morphology of the active layer. When DAD is added to the casting solvent, P3HT crystallization is increasing and leads to a significant enhancement of Jsc and FF values (Figure 2). PCE reachs its maximum values of 2.8% for 1 vol.% of DAD. If too much additive is used, device performances decrease due to a reduced FF and Jsc. Furthermore, atomic force microscopy confirmed the same typical structured morphology at the nanoscale of P3HT:$PC_{61}BM$ processed with optimized content of DAD or ODT (Figure 3). The films with 1,10-diazidodecane exhibit a root mean square of 11 nm (Figure 3i), while the film with OT exhibits the RMS of 13 nm (Figure 3g).
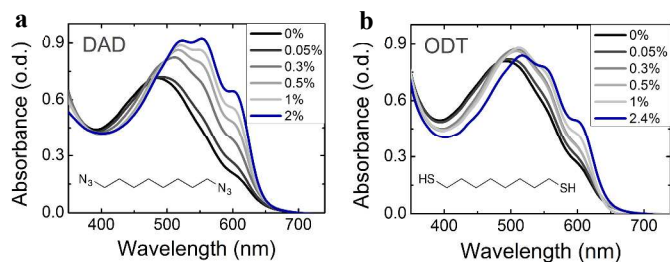

Figure 1 – UV-Visible spectroscopy. Absorption of P3HT:$PC_{61}BM$ composite layer processed with various volume ratio of (a) 1,10-diazidodecane and (b) 1,8-octanedithiol.

The stabilization effect of DAD on morphology based on P3HT:$PC_{61}BM$ upon accelerated ageing (at 150°C) was followed by optical microscopy and AFM. Figure 3a shows P3HT:$PC_{61}BM$ layers processed without additive. After 24 hours at 150°C, micro-phase separation occurs and the entire surface is covered with $PC_{61}BM$ crystals (Figure 3b). In contrast, the addition of DAD into P3HT:$PC_{61}BM$ solution inhibits the formation of $PC_{61}BM$ clusters for 2 vol. % of DAD added (Figure 3c-f). After 24 hours at 150°C, the pristine phase image of P3HT:$PC_{61}BM$ bulk heterojunction completely changes due to $PC_{61}BM$ crystallization (Figure 3g-h) whereas the addition of 2 vol. % of DAD allows the stabilization of the morphology (Figure 3i-j). FTIR spectroscopy confirmed the cycloaddition reaction between DAD and $PC_{61}BM$. Figure S2 depicts the Infrared spectra in transmission mode of a P3HT:$PC_{61}BM$ composite layer processed with 2 vol. % of DAD on sapphire substrates before and after cross-linking activation (10 min at 150°C). The spectra show the presence of the thiophene ring vibration at 3057 cm^{-1}, as well as signatures of aliphatic side chains of P3HT and of the DAD ($\nu_{asym}CH_3$ and $\nu_{asym}CH_2$ at 2957 and 2924 cm^{-1} respectively, and $\nu_{sym}CH_2$ at 2852 cm^{-1}). After treatment reaction at 150 °C, the intensity of the peak at 2092 cm^{-1}, attributed to the azide functional groups, is significantly reduced, indicative of the reaction of N_3.

To examine the effect of DAD on the thermal stability of device performance, P3HT:$PC_{61}BM$ based solar cells processed with 2% of DAD and 2.4% of ODT were compared before and after thermal ageing at 150°C during 24 hours. The current-voltage (J-V) curves of these solar devices are plotted in Figure S1. Pristine solar cells processed with ODT exhibited power conversion efficiency of 2.8% compared to 1.9% with DAD. This difference could be explain by a non-optimal ratio of DAD added which will be discussed in the following section. A volume ratio of 2% is chosen here to highlight the thermal stabilization effect of DAD by optical microscopy observation (Figure 3f). Indeed, after a thermal ageing at 150°C during 24 hours, performances of ODT-based devices dropped from 2.8% to 0.2% due to micro-phase separation between P3HT and $PC_{61}BM$ (Figure 3b). In contrast, solar cells incorporating DAD displayed stabilized efficiency at 2.5% after the same thermal treatment thanks to the inhibition of fullerene micro-crystallization inside the active layer.
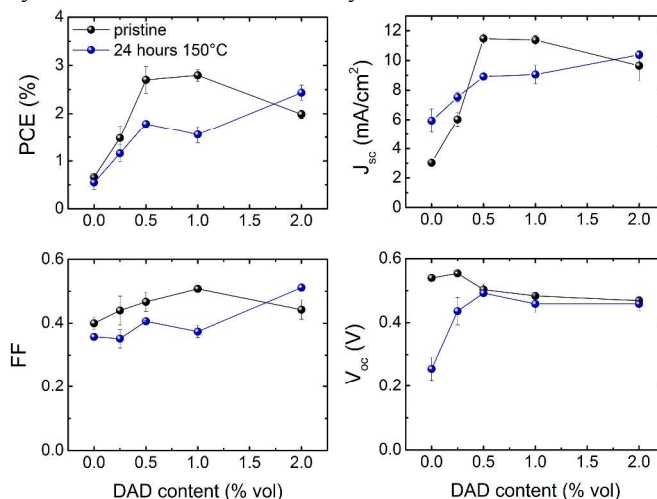

Figure 2 – Photovoltaic performances of P3HT:$PC_{61}BM$ solar cells embedding DAD in various concentrations a) pristine (black symbols) and b) after 24 hours at 150°C (blue symbols).

After thermal ageing (blue symbols on Figure 2), pristine P3HT:$PC_{61}BM$ solar cells show micro-sized crystals of $PC_{61}BM$ covering the entire surface (Figure 3b). This micro-phase separation leads in poor device performances with a corresponding efficiency of 0.5%. However, when 2 vol. % of DAD is added, cross-linking activation avoid micro-crystal formation after the same thermal ageing (Figure 3f-j). Hence, devices efficiencies are stabilized at 2.5 % by locking the P3HT:$PC_{61}BM$ network morphology (Figure 3f-j). Below this concentration, the amount of cross-linker is not enough to entirely inhibit $PC_{61}BM$ clusters formation (Figure 3c-e). As a consequence, one can see that the optimized concentration of DAD depends on the properties one is looking for. To summarize, on the first hand, achieving optimized initial PCE values requires the use of 1% of DAD but does not lead to the most optimized stabilization of BHJ morphology. On the other hand, increasing DAD content up to 2% enables to achieve slightly lower initial PCE but highly stabilized morphology.
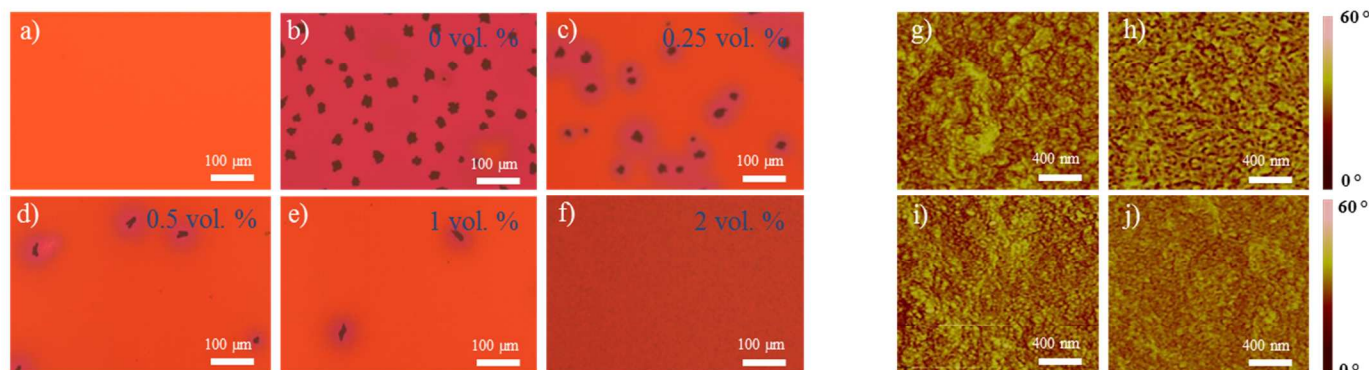
Journal Name

Figure 3 – Optical microscopy. P3HT:PC$_{61}$BM layers (a) pristine (b-f) after 24 hours at 150°C as function of 1,10-diazidodecane vol. ratio added in the solution. AFM phase images of P3HT:PC$_{61}$BM layer processed with 2,4 vol. % ODT (g) as-cast and (h) after thermal ageing at 150°C during 24 hours. AFM phase images of P3HT:PC$_{61}$BM layer processed with 2 vol. % of DAD (i) as-cast and (j) after 24 hours at 150°C.

There is clearly a compromise to deal with concerning additive content to achieve both effects morphology enhancement and crosslinking stabilization. In conclusion, a new bis-azide molecule is applied as cross-linkable additive to enhance initial photovoltaic performances of P3HT:PC$_{61}$BM solar cells and stabilize thermally the morphology. We demonstrated here that the incorporation of 1,10-diazidodecane (DAD) into P3HT:PC$_{61}$BM blend leads to an appropriate nano-scaled phase separation similar to the one obtained with the use of 1,8-octanedithiol as a reference solvent additive.

Hence, solar cells power conversion efficiency based on films coated with an optimal ratio of DAD is enhanced from 0.6% to 2.8%. Furthermore, cross-linking activation of our additive inhibits PC$_{61}$BM clusters formation during prolonged thermal ageing. Photovoltaic performances of solar cells with DAD are stabilized at 2.6% after 24 hours at 150°C whereas P3HT:PC$_{61}$BM:ODT based reference devices decrease rapidly to 0.66% respectively after the same thermal ageing. This study demonstrates that solvent additives commonly used to tune BHJ active layer morphology can be easily made functional to also enhance the stability of layers versus thermal stresses by crosslinking. Further research is under progress to extend this concept of double effect additive to other polymer:fullerene blends, especially with state-of-the-art low band-gap polymers which usually require a solvent additive process to display optimal performances.

Notes and references

[1] G. Yu, J. Gao, J. C. Hummelen, F. Wudl and A. J. Heeger, *Science*, 1995, **270**, 1789-1791.

[2] A. J. Heeger, *Advanced Materials*, 2014, **26**, 10-28.

[3] G. Li, V. Shrotriya, J. Huang, Y. Yao, T. Moriarty, K. Emery and Y. Yang, *Nature Materials*, 2005, **4**, 864-868.

[4] J. Peet, J. Y. Kim, N. E. Coates, W. L. Ma, D. Moses, A. J. Heeger and G.C. Bazan, *Nature Materials*, 2007, **6**, 497-500.

[5] U. Vongsaysy, B. Pavageau, G. Wantz, D. M. Bassani, L. Servant, H. Aziz, Advanced Energy Materials, 2014, **4**, 1-9.

[6] T. Salim, L. H. Wong, B. Bräuer, R. Kukreja, Y. L. Foo, Z. Bao and Y. M. Lam, *J. Mater. Chem*, 2011, **21**, 242-250.

[7] H.-C. Liao, C.-C. Ho, C.-Y. Chang, M.-H. Jao, S. B. Darling and W.-F. Su, *Materialstoday*, 2013, **16**, 326-336.

[8] U. Vongsaysy, D. Bassani, L. Servant, B. Pavageau, G. Wantz, H. Aziz, *Journal of Photonics for Energy*, 2014, accepted

[9] M.T. Dang, L. Hirsch and G. Wantz, *Advanced Materials*, 2011, **23**, 3597-3602.

[10] A. Pivrikas, P. Stadler, H. Neugebauer, N. S. Sariciftci, *Organic Electronics*, 2008, **5**, 775–782.

[11] Y. Yao, J. Hou, Z. Xu, G. Li and Y. Yang, *Advanced Function Materials*, 2008, **18**, 1783-1789.

[12] O. Oklobia, T.S. Shafai, *Solar Energy Materials & Solar Cells*, 2013, **117**, 1-8.

[13] C. Lindqvist, A. Sanz-Velasco, E. Wang, O. Bäcke, S. Gustafsson, E. Olsson, M. R. Andersson and C. Müller, *Journal of Materials Chemistry A*, 2013, **1**, 7174.

[14] A. Swinnen, I. Haeldermans, M. vande Ven, J. D'Haen, G. Vanhoyland, S. Aresu, M. D'Olieslaeger and J. Manca, *Advanced Functional Materials*, 2006, **16**, 760-765.

[15] L. Derue, O. Dautel, A. Tournebize, M. Drees, H. Pan, S. Berthumeyrie, B. Pavageau, E. Cloutet, S. Chambon, L. Hirsch, A. Rivaton, P. Hudhomme, A. Facchetti and G. Wantz, *Advanced Materials*, 2014, **26**, 5831-5838.

[16] M. O. Reese, S. A. Gevorgyan, M. JØrgensen, E. Bundgaard, S. R. Kurtz, D. S. Ginley, D. C. Olson, M. T. Lloyd, P. Morvillo, E. A. Katz, A. Elschner, O. Haillant, T. R. Currier, V. Shrotriya, M. Hermenau, M. Riede, K. R. Kirov, G. Trimmel, T. Rath, O. Inganäs, F. Zhanf, M. Andersson, K. Tvingstedt, M. Lira-Cantu, D. Laird, C. McGuiness, S. Gowrisanker, M. Pannone, M. Xiao, J. Hauch, R. Steim, D. M. DeLongchamp, R. Rösch, H. Hoppe, N. Espinosa, A. Urbina, G. Yaman-Uzunoglu, J.-B. Bonekamp, A. J.J.M. van Breemen, C. Girotto, E. Voroshazi, F. C. Krebs, *Solar Energy Materials & Solar Cells*, 2011, **95**, 1253-1267.

[17] G. Wantz, L. Derue, O. Dautel, A. Rivaton, P . Hudhomme and C. Dagron-Lartigau, *Polymer international*, 2014, **63**, 1346-1361.

[18] A. Charas, Q. Ferreira, J. Farinhas, M. Matos, L. Alcacer and J. Morgado, *Macromolecules*, 2009, **42**, 7903-7912.

[19] B. J. Kim, Y. Miyamoto, B. Ma and J.M.J. Fréchet, *Advanced Functional Materials*, 2009, **19**, 2273-2281.

[20] S. Khiev, L. Derue, G. Ayenew, H. Medlej, R. Brown, L. Rubatat, R.C. Hiorns, G. Wantz and C. Dagron-Lartigau, *Polymer Chemistry*, 2013, **4**, 4145-4150.

[21] S. Bertho, B. Campo, F. Piersimoni, D. Spoltore, J. D'Haen, L. Lutsen, W. Maes, D. Vanderzande and J. Manca, *Solar Energy Materials & Solar Cells*, 2013, **110**, 69-73.

22 H.J. Kim, R. Han, C.-H. Cho, H. Kang, H.-H. Cho, M.Y. Lee, J.M.J. Fréchet, J. H. Oh and B. J. Kim, *Chemical materials*, 2012, **24**, 215-221.
23 G. Li, V. Shrotriya, Y. Yao, J. Huang, Y. Yang, *Journal of Materials Chemistry*, 2007, **17**, 3126-3140.

RSC Advances Accepted Manuscript